International Immunopharmacology 74 (2019) 105724

Contents lists available at ScienceDirect

International Immunopharmacology

journal homepage: www.elsevier.com/locate/intimp

Autoinducer-2 of *Fusobacterium nucleatum* promotes macrophage M1 polarization *via* TNFSF9/IL-1β signaling

Jiao Wu[a,1], Kang Li[b,1], Wei Peng[a], Huan Li[a], Qing Li[a], Xianfei Wang[c], Yan Peng[a], Xiaowei Tang[a], Xiangsheng Fu[c,*]

[a] Department of Gastroenterology, the Affiliated Hospital of Southwest Medical University, Sichuan 646000, China
[b] High Altitude Medical Research Institute, People's Hospital of Tibet Autonomous Region, Lhasa 850000, China
[c] Department of Gastroenterology, The Affiliated Hospital of North Sichuan Medical College, Sichuan 637000, China

ARTICLE INFO

Keywords:
Autoinducer-2
Colorectal cancer
Fusobacterium nucleatum
Gut microbiota
Macrophages

ABSTRACT

The effect of *Fusobacterium nucleatum* (*F. nucleatum*) autoinducer-2 (AI-2) on the polarization of macrophages and the underlying mechanism is not known. We investigated the effect of *F. nucleatum* AI-2 on the migration and polarization of cultured macrophages. We further screened AI-2-interacting proteins in macrophages using a quantitative proteomics strategy, and evaluated the expression of TNFSF9/TRAF1/p-AKT/IL-1β signaling in cultured macrophages and human colorectal cancer (CRC). The data showed that *F. nucleatum* AI-2 enhanced the mobility and M1 polarization of macrophages, possibly through TNFSF9/TRAF1/p-AKT/IL-1β signaling. Moreover, TNFSF9 and IL-1β expression was significantly increased in human CRCs when compared to normal colon ($P < 0.05$), and was associated with AI-2 concentration and increased survival. Together, our data suggested that AI-2 induced macrophage M1 polarization by activating the TNFSF9/IL-1β pathway. Thus, AI-2 may serve as a promising novel target for immunotherapy of gut microbiota-related diseases.

1. Introduction

The mammalian gut is home to a large population of microorganisms, where host and microorganisms coordinate with each other to maintain homeostasis [1]. The co-evolution of animals with their gut microbiota has formed a precise balance [2]. An imbalance among gut microbiota or between host and resident microbiota can lead to a variety of diseases, including obesity [3], diabetes [4], cardiovascular atherosclerosis [5], Parkinson's and neurodegenerative diseases, inflammatory bowel disease (IBD), and colorectal cancer (CRC) [6]. Therefore, communication between gut microbiota and the host is of utmost importance for homeostasis of host physiology and health [7]. However, currently, the underlying mechanism of action between gut microbiota and the gut is not well understood.

Found in large numbers of gram-positive and gram-negative bacteria, the quorum sensing (QS) system is an important mechanism both within and between species, and enables bacteria to act as a team rather than as a single cell [8]. QS plays an important role in bacterial cell density, biofilm formation, virulence, and antibiotic production [9]. Autoinducer-2 (AI-2) is a major signal-type molecule of QS, and is a nonspecies-specific autoinducer that is involved in mediating communication among interspecies [10]. AI-2 can mediate bacterial colonization in the intestinal tract, thereby changing the composition of intestinal bacteria, and regulating the host immune response, leading to intestinal diseases [10]. In a previous study, it was reported that AI-2 synthetase (LuxS) can affect the host's pro-inflammatory responses to *Porphyromonas gingivalis* [11]. Thus, it is conceivable that AI-2 can be sensed by the host's immune system.

As an important barrier against pathogen invasion, macrophages play a critical role in microbial sensing, inflammatory disease, and cancer [12]. The heterogeneity of macrophages can be shaped based on the microenvironment [13]. For example, in the tumor microenvironment, macrophages can differentiate into distinct functional phenotypes that range from M1-phenotype to M2-phenotype [14]. The main effect of M1 type polarization is pro-inflammatory, and mainly mediates the release of inflammatory cytokines, including IL-1β, IL-8, and TNF-α. M2 type polarization is anti-inflammatory and tumor-promoting, and mainly mediates the release of cytokines, such as TGF-β, IL-10, and IL-4 [15]. However, whether AI-2 can shape the polarization of macrophages has never been investigated before.

* Corresponding author at: Department of Gastroenterology, The Affiliated Hospital of North Sichuan Medical College, Road Wenhua 63#, Region Shunqing, Sichuan 637000, China.
E-mail address: drfuxs@gmail.com (X. Fu).
[1] These authors contributed equally to this work.

https://doi.org/10.1016/j.intimp.2019.105724
Received 30 March 2019; Received in revised form 11 June 2019; Accepted 25 June 2019
Available online 01 July 2019
1567-5769/

Recently, *Fusobacterium nucleatum* (*F. nucleatum*) has been found to play an important role in the development of intestinal inflammatory diseases and CRC [16]. Molecules of *F. nucleatum*, such as lipopolysaccharide (LPS), FadA, Fap2, and RadD, can invade the mucosal epithelium, and stimulate the release of inflammatory factors, such as NF-κB, IL-6, IL-8, IL-10, and IL-18, thereby creating an inflammatory microenvironment that favors the development of CRC [17]. Moreover, inflammatory signaling pathways play an important role in the initiation and development of CRC [18]. For example, AKT/IL-1β and ERK/IL-6 signaling form important molecular bases for the secretion of inflammatory factors, and are aberrantly activated in CRCs [19,20]. However, the effect of *F. nucleatum* AI-2 on the release of inflammatory factors in macrophages as well as the underlying mechanism involved has never been investigated.

We hypothesized that AI-2 from *F. nucleatum* can shape the phenotype of macrophages. Therefore, in the present study, we explored whether *F. nucleatum* AI-2 plays a role on the migration and polarization of macrophages. We further screened AI-2-interacting proteins in cultured macrophages using a quantitative proteomics approach. Our findings showed that AI-2 activated TNFSF9/TRAF1/P-AKT/IL-1β signaling in macrophages *in vitro*. Moreover, the expression of TNFSF9 and IL-1β was upregulated in human CRC tissues, and was associated with increased survival. Combined, our data provided a novel therapeutic target for gut microbiota-related diseases.

2. Materials and methods

2.1. Sample collection and bacterial culture

Both stool and CRC tissue samples were collected from 40 CRC patients admitted to the Affiliated Hospital of Southwest Medical University (Sichuan, China) between February 2017 and December 2017. Exclusion criteria included use of antibiotic within 3 months of study participation, inflammatory diseases, familial polyposis syndrome, pregnancy and radiation [21]. Informed consent was obtained from all participants and the study was approved by the review board of the Affiliated Hospital of Southwest Medical University.

In brief, stool samples were prepared as described by Raut. et al., and each sample was weighed and suspended, then diluted with steriled water to a final dilution of 1:750 (w/v) [22]. Tumor tissues were fixed in 4% paraformaldehyde and embedded in paraffin for immunofluorescence analysis.

F. nucleatum (*F01*) strains were isolated from a proximal colon cancer tissue as described in our previous study [23]. *F. nucleatum* were cultured in fastidious anaerobe broth (FAB) medium containing 10% serum in a humidified anaerobic chamber (85% N_2, 10% H_2, and 5% CO_2 at 37 °C). The AI-2 reporter strain *Vibrio harveyi* (*V. harveyi*) BB170 was purchased from the Guangdong culture collection center (Guangzhou, China), and was cultured in autoinducer bioassay (AB) medium at 30 °C as previously described [24].

2.2. Purification of F. nucleatum AI-2

Purification of *F. nucleatum* AI-2 was demonstrated as previously described [25]. Briefly, an overnight culture of *F. nucleatum* was diluted 1:10 with fresh AB medium and cultured at 37 °C until the late exponential phase (OD660 nm = 0.7). Culture supernatants were prepared by centrifugation at 10,000 × *g*, transferred to 0.2 μm-pore-size membrane filters, and subsequently passed through a Centricon YM-3 3-kDa exclusion filter. The filtrate was lyophilized, and a small amount (200 mg) was dissolved in 2 mL of cold buffer solution (pH 6.2), and chromatographed on a C18 Sep-Pak reverse-phase column (Waters Co., Milford, MA, USA) according to the manufacturer's instructions.

2.3. Determination of AI-2-mediated bioluminescence

V. harveyi strain BB170 was inoculated in AB medium at 30 °C with aeration until OD600 = 0.7. Then, the strain was diluted with fresh AB medium at a ratio of 1:5000. The bacterial suspension was mixed with purified *F. nucleatum* AI-2 or AI-2 and its inhibitor D-ribose (50 μM) (Tokyo Chemical Industry Co. Tokyo, Japan) at a final concentration of 10% (vol/vol) and incubated for 6 h at 30 °C. Stool samples were processed as described above. Ten microliter of each of the processed samples was added in triplicate to 90 μL of diluted *V. harveyi* BB170 cultures in 96-well polystyrene microtiter plates (Costar, corning, NY, USA).

Bioluminescence was recorded by a TriStar LB 941 microplate reader (Berthold, Wildbad, Germany). The standard solution 4,5-dihydroxy-2,3-pentanedione (DPD) (the precursor of AI-2, Omm Scientific Inc. CAS: 142937-55-1) was diluted with sterile water to concentrations of 1000, 100, 10, and 1 μmol/L, and 100, 10, 1, and 0.1 nmol/L. Then, an AI-2 quantitative detection standard curve was established as previously described [22]. Nonlinear regression analysis [log (agonist) *vs* response - variable slope] was used for the analysis of dose-response curves, and the concentration of AI-2 was calculated based on the bioluminescence value.

2.4. Cell culture and differentiation induction

U937 cells were purchased from the American Type Culture Collection (Manassas, VA, USA) and maintained in Gibco RPMI1640, supplemented with 10% (v/v) fetal calf serum and 1% (v/v) penicillin G/streptomycin at 37 °C under 5% CO_2. For all experiments, U937 cells were differentiated to obtain a macrophage-like phenotype by addition of phorbol 12-myristate 13-acetate (PMA) (Sigma-Aldrich, St. Louis, MO, USA) at 100 ng/mL, at 37 °C for 48 h [26].

2.5. High-throughput quantitative proteomic analysis

U937 cells induced by PMA were treated with *F. nucleatum* AI-2 or an equal amount of cell culture medium as a control. Proteins were isolated and digested from AI-2-treated cells and controls. After digestion, peptides were processed and analyzed as previously described [27]. Differentially expressed proteins were identified using a cutoff of absolute fold change of ≥ 1.3. The gene ontology (GO) enrichment test with $P < 0.05$ was considered significant. Experiments were performed in triplicate.

2.6. Cell migration assay

For quantitative cell migration assays, chambers (Corning, Tewksbury, MA, USA) with 8.0-μm polycarbonate filter inserted in 24-well plates were used. U937 cells induced by PMA (1×10^5 cells/well) were added in the upper chamber and the lower chambers were filled with four different treatments: complete medium containing 20% serum (CTR), CTR + AI-2 (400 μM), CTR + AI-2 (50 μM), and CTR + AI-2 (400 μM) + D-ribose (50 μM). The 24-well plates containing cells were placed in a thermostatic incubator at 37 °C for 16 h. Then, the transferred cells were fixed with 4% paraformaldehyde, stained with crystal violet, and counted using an inverted microscope (IX73; Olympus, Tokyo, Japan). Experiments were performed in triplicate.

2.7. Quantitative real-time PCR analysis of M1/M2-polarized macrophages

Equal amounts of PMA-stimulated U937 cells (1×10^6) were treated with AI-2 (50 μM), AI-2 (400 μM), AI-2 (400 μM) + D-ribose (50 μM), and an equal amount of cell culture medium (control). After 6 h, total RNA was extracted using an RNA extraction kit (TIANGEN, China). A Reverse Transcription kit (TOYOBO, Japan) was used to

prepare cDNA and quantitative real-time PCR was performed using QuantiNovaTM SYBR Green PCR Kit (Qiagen, Germany) on an Applied Biosystems StepOnePlus Real-Time PCR system. The primers used are presented in Supplementary Table S1.

2.8. Western blot analysis

Total cellular protein was extracted from cultured cells using a protein extraction solution (Beyotime, China). Western blot analysis was performed as previously described [14]. Primary antibodies used in this study were as follows: anti-GAPDH (1:10,000; Bioworld), anti-p-ERK1/2 (1:1000; Beyotime), anti-p-AKT (1:1000; Beyotime), anti-IL-1β (1:1000; Bioworld), anti-TRAF1 (1:1000; Proteintech), anti-IL-6 (1:1000; Bioworld), anti-TNFSF9 (1:1000; Bioworld). Membranes were then incubated with the appropriate secondary antibodies for 1 h at room temperature. Membranes were analyzed using Quantity One 4.5.0 software (Bio-Rad Laboratories, CA, USA). Experiments were performed in triplicate.

2.9. Immunofluorescence

Immunofluorescence staining was performed using formalin-fixed, paraffin-embedded tissue sections as described in our previous study [14]. The primary antibodies used for immunofluorescence were as follows: anti-CD68 (1:100, Santa Cruz, CA, USA); anti-TNFSF9 (1:100, Bioworld, USA); anti-IL-1β (1:100, Bioworld, USA). Each section was incubated with appropriate secondary antibodies: FITC-labeled goat anti-mouse IgG (1:200, Beyotime, China), Cy3-labeled goat anti-rabbit IgG (1:500, Beyotime, China) for 1 h at 37 °C. DAPI (Beyotime, China) was used for nuclear counterstain at room temperature for 10 min. Images were captured using a microscope (BX53; Olympus, Tokyo, Japan). Immunofluorescence for macrophage markers CD68 and proteins (TNFSF9 and IL-1β) was determined from captured pictures. A total of five random fields at 400× magnification were captured for each sample, and positive cells were presented as an average number of positive cells per square millimeter.

2.10. Statistical analysis

Data are presented as the mean and standard deviation for continuous variables and as proportions for categorical variables. Data were analyzed using one-way ANOVA, followed by the Bonferroni test for multiple comparisons. All significance tests were two-tailed. Statistical analysis was performed using SPSS software version 13.0 (SPSS Inc., Chicago, IL, USA). $P < 0.05$ was considered significant.

3. Results

3.1. AI-2 activity of F. nucleatum

As shown in Fig. 1A, a standard curve was obtained from bioluminescence values corresponding to different AI-2 concentration gradients. According to nonlinear regression analysis, the concentration of AI-2 purified from *F. nucleatum* (*F01*) was 251.7 μmol/L. Moreover, AI-2 purified from *F. nucleatum* (*F01*) significantly induced bioluminescence when compared to the untreated control group ($P < 0.0001$) (Fig. 1B). In addition, AI-2 inhibitor D-ribose significantly inhibited AI-2-induced bioluminescence ($P < 0.0001$) (Fig. 1B).

3.2. AI-2 of F. nucleatum promoted macrophage migration and M1 polarization

We compared the migration ability of U937-derived macrophages treated with *F. nucleatum* AI-2 and untreated macrophages using transwell assays. U937-derived macrophages treated with AI-2 at both low concentration (50 μM) and high concentration (400 μM) showed an increase in migration when compared to untreated macrophages (both P values < 0.0001). In addition, AI-2 inhibitor D-ribose significantly attenuated the migration of macrophages induced by AI-2 ($P < 0.0001$) (Fig. 2A, B). Combined, these findings demonstrated that *F. nucleatum* AI-2 enhanced the mobility of human macrophages.

Since the phenotype of macrophages determines the immune response to bacterium infection, we further examined the mRNA levels of both macrophage M1 markers (IL-8, TNF-α and IL-1β), and M2 markers (IL-10 and TGF-β) by qPCR after AI-2 challenge. We found that M1 markers, such as IL-8, TNF-α, and IL-1β were expressed at a significantly higher level at high concentration (400 μM) of AI-2-challenged U937-derived macrophages when compared to the control group (all P values < 0.0001). These induction effects were significantly blocked by AI-2 inhibitor D-ribose (all P values < 0.0001). However, the levels of TGF-β did not significantly change after AI-2 treatment ($P > 0.05$). IL-10 was expressed at a significantly lower level in AI-2-challenged macrophages when compared to the control group ($P < 0.0001$) (Fig. 2C, D). AI-2 inhibitor D-ribose did not significantly influence the levels of M2 markers (IL-10 and TGF-β) of AI-2-challenged macrophages. Together, these results suggested that *F. nucleatum* AI-2 promoted the differentiation of M1 macrophages.

3.3. AI-2 induced high expression of cytokine-cytokine receptor interaction including TNFSF9 signaling in U937-derived macrophages

AI-2-interacting proteins in U937-derived macrophages were analyzed using a quantitative proteomics approach. As a result, 5927 protein groups were identified, among which 5317 proteins were quantified. Among the 5317 genes, there were 57 genes with an expression level > 1.3-fold change. Forty-six proteins were up-regulated and 11 proteins were down-regulated (Table 1). The 46 up-regulated proteins primarily induced expression of cytokines, such as TNFSF9, IL-1β, C-C motif chemokine (CCL20), PTGS2, TRAF1, and C-C motif chemokine 3 (CCL3). Importantly, the most differentially upregulated proteins included TNFSF9 (3.621-fold) and IL-1β (3.045-fold).

To evaluate the biological relevance of AI-2 with U937-derived macrophages, cluster analysis was performed to create a heat-map, which contained the data obtained for the 5317 dysregulated proteins. The results showed that 46 up-regulated proteins were classified as involved in response to bacteria, responses to the molecule of bacterial origin, regulation of inflammatory response, and cell migration (Fig. 3A). Kyoto Encyclopedia of Genes and Genomes (KEGG) analysis revealed that AI-2 treatment activated 26 significant pathways ($P < 0.05$). The top four activated pathways included cytokine-cytokine receptor interaction, rheumatoid arthritis, the IL-17 signaling pathway, and the TNF signaling pathway (Fig. 3B, C). The more prominent proteins TNFSF9, IL-1β, CCL-20, PTGS2, and TRAF1 were mainly concentrated in the TNF signaling pathway, thus may induce M1 polarization of macrophages.

3.4. AI-2 activated TNFSF9/TRAF1/P-AKT/IL-1β signaling in U937-derived macrophages in vitro

To delineate the molecular mechanisms by which AI-2 induced macrophage M1 polarization, TNFSF9/TRAF1/p-AKT/IL-1β and p-ERK/IL-6 signaling were further investigated by Western blot analysis in cultured macrophages that were challenged with *F. nucleatum* AI-2. When compared to the control group, the expression of TNFSF9, TRAF1, p-AKT, and IL-1β was significantly increased in cultured U937-derived macrophages after AI-2 challenge at both 50 μM and 400 μM (all P values < 0.05). D-ribose pre-treatment before AI-2 challenge (400 μM) significantly decreased the expression of TNFSF9, TRAF1, p-AKT and IL-1β (all P values < 0.05) (Fig. 4A, B). However, when compared to the control group, p-ERK expression did not significantly change, and IL-6 expression significantly decreased after AI-2 challenge ($P < 0.05$). Furthermore, the positive control LPS significantly

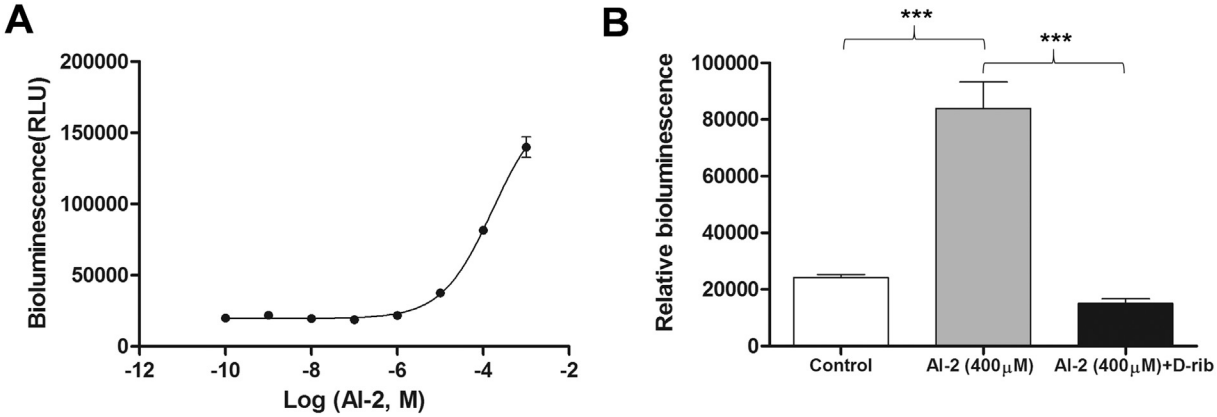

Fig. 1. Establishment of a standard curve for AI-2 quantitative detection and bioluminescence activity of AI-2 purified from *Fusobacterium nucleatum*. (A) The standard curve of relative light induction and the log10 of the calculable AI-2 concentration. (B) *Fusobacterium nucleatum* AI-2 (400 μM) significantly induced bioluminescence when compared to the untreated control group. D-ribose (50 μM) pre-treatment significantly decreased the bioluminescence. $^{***}P < 0.0001$. AI-2, autoinducer-2; D-rib, D-ribose.

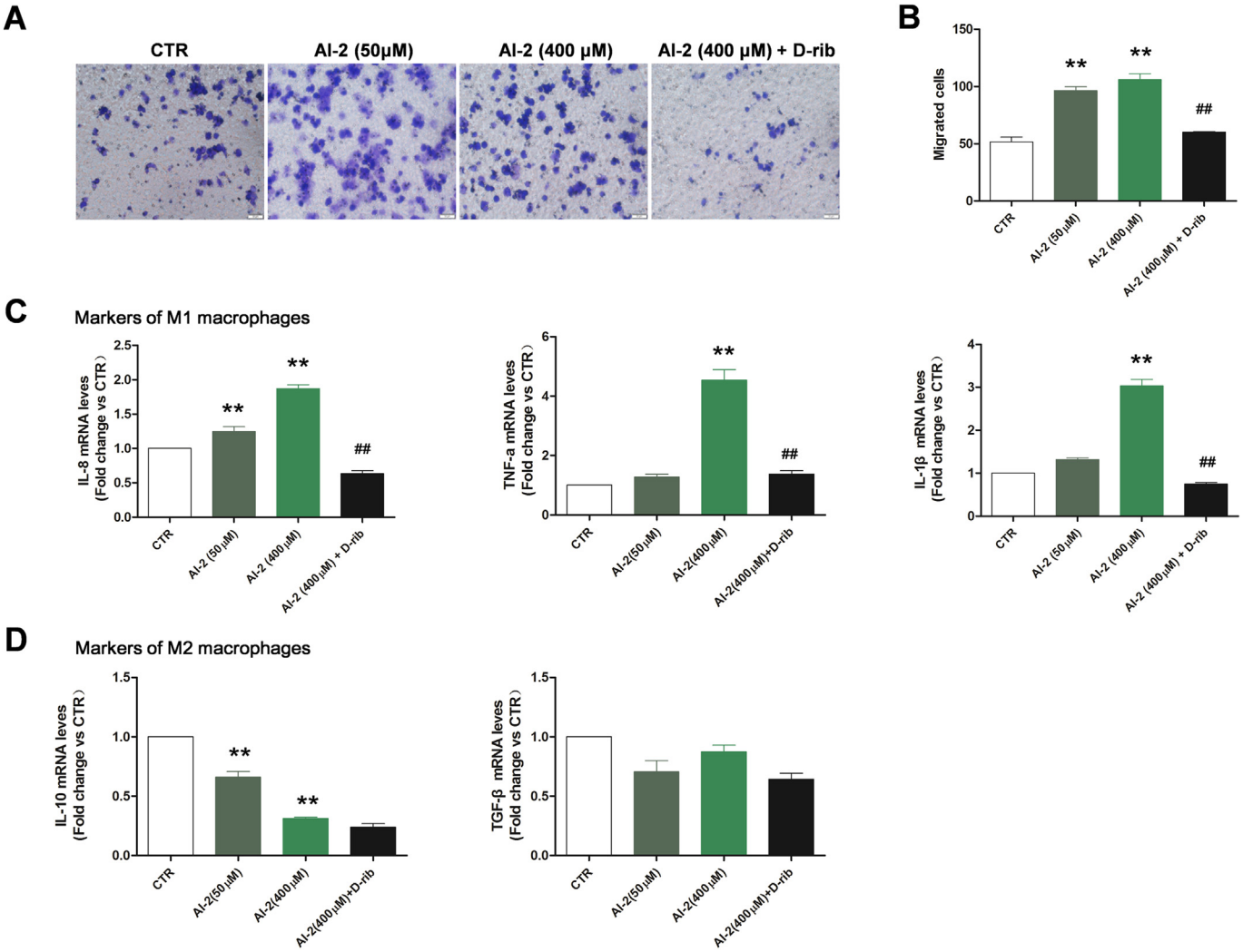

Fig. 2. *Fusobacterium nucleatum* AI-2 favors migration and M1 polarization of cultured U937-derived macrophages. (A, B) AI-2 purified from *Fusobacterium nucleatum* at both low concentration (50 μM) and high concentration (400 μM) significantly increased migration of macrophages. Pre-treatment with D-ribose (50 μM) significantly decreased the migration of macrophages. (C) M1 macrophages markers (IL-8, TNF-α, and IL-1β) were significantly increased in macrophages that were challenged with a high concentration (400 μM) of AI-2 when compared to the control group. Pre-treatment with D-ribose decreased macrophage M1 polarization. (D) M2 macrophage marker IL-10 was significantly decreased in AI-2 challenged macrophages when compared to the control group. TGF-β expression did not significantly change after AI-2 treatment. $^{**}P < 0.0001$ compared to the control group. $^{\#\#}P < 0.0001$ compared to the AI-2 (400 μM) group. CTR, control; AI-2, autoinducer-2; D-rib, D-ribose.

Table 1
Proteins with at least 1.3-fold change in abundance in AI-2 treated U973-derived macrophages compared with control.

Protein accession	Gene name	Protein description	AI-2/control Ratio	AI-2/control *P* value	Regulated type
P41273	TNFSF9	Tumor necrosis factor ligand superfamily member 9 OS = Homo sapiens OX = 9606 GN = TNFSF9	3.621	0.0019838	Up
P35354	PTGS2	Prostaglandin G/H synthase 2 OS = Homo sapiens OX = 9606 GN = PTGS2	3.551	0.00014238	Up
P01584	IL1B	Interleukin-1 beta OS = Homo sapiens OX = 9606 GN = IL1B	3.045	0.00063738	Up
Q702N8	XIRP1	Xin actin-binding repeat-containing protein 1 OS = Homo sapiens OX = 9606 GN = XIRP1	2.307	0.010498	Up
P05121	SERPINE1	Plasminogen activator inhibitor 1 OS = Homo sapiens OX = 9606 GN = SERPINE1	2.282	0.0014379	Up
P78556	CCL20	C-C motif chemokine 20 OS = Homo sapiens OX = 9606 GN = CCL20	2.168	0.0001382	Up
P10147	CCL3	C-C motif chemokine 3 OS = Homo sapiens OX = 9606 GN = CCL3	2.166	0.0079787	Up
Q02487	DSC2	Desmocollin-2 OS = Homo sapiens OX = 9606 GN = DSC2	2.045	0.0094607	Up
O15492	RGS16	Regulator of G-protein signaling 16 OS = Homo sapiens OX = 9606 GN = RGS16	2.007	0.00091878	Up
P05120	SERPINB2	Plasminogen activator inhibitor 2 OS = Homo sapiens OX = 9606 GN = SERPINB2	1.781	0.0036788	Up
Q9NYS0	NKIRAS1	NF-kappa-B inhibitor-interacting Ras-like protein 1 OS = Homo sapiens OX = 9606 GN = NKIRAS1	1.699	0.00020496	Up
P38936	CDKN1A	Cyclin-dependent kinase inhibitor 1 OS = Homo sapiens OX = 9606 GN = CDKN1A	1.693	0.00023895	Up
Q99541	PLIN2	Perilipin-2 OS = Homo sapiens OX = 9606 GN = PLIN2	1.668	0.0046628	Up
P01100	FOS	Proto-oncogene c-Fos OS = Homo sapiens OX = 9606 GN = FOS	1.652	0.00012019	Up
Q07352	ZFP36L1	mRNA decay activator protein ZFP36L1 OS = Homo sapiens OX = 9606 GN = ZFP36L1	1.651	0.0044219	Up
O43918	AIRE	Autoimmune regulator OS = Homo sapiens OX = 9606 GN = AIRE	1.647	4.4147E-05	Up
Q9ULX9	MAFF	Transcription factor MafF OS = Homo sapiens OX = 9606 GN = MAFF	1.641	0.0153829	Up
Q9H7S9	ZNF703	Zinc finger protein 703 OS = Homo sapiens OX = 9606 GN = ZNF703	1.638	7.6885E-05	Up
O14763	TNFRSF10B	Tumor necrosis factor receptor superfamily member 10B OS = Homo sapiens OX = 9606 GN = TNFRSF10B	1.574	0.0023187	Up
Q13077	TRAF1	TNF receptor-associated factor 1 OS = Homo sapiens OX = 9606 GN = TRAF1	1.567	0.0023622	Up
O00175	CCL24	C-C motif chemokine 24 OS = Homo sapiens OX = 9606 GN = CCL24	1.556	0.030536	Up
Q9UNW9	NOVA2	RNA-binding protein Nova-2 OS = Homo sapiens OX = 9606 GN = NOVA2	1.553	0.0020974	Up
P03956	MMP1	Interstitial collagenase OS = Homo sapiens OX = 9606 GN = MMP1	1.528	0.0028611	Up
P11169	SLC2A3	"Solute carrier family 2, facilitated glucose transporter member 3 OS = Homo sapiens OX = 9606 GN = SLC2A3"	1.508	0.0037227	Up
Q9HBL0	TNS1	Tensin-1 OS = Homo sapiens OX = 9606 GN = TNS1	1.485	0.0085022	Up
Q16548	BCL2A1	Bcl-2-related protein A1 OS = Homo sapiens OX = 9606 GN = BCL2A1	1.485	0.00095749	Up
Q01151	CD83	CD83 antigen OS = Homo sapiens OX = 9606 GN = CD83	1.485	0.0090408	Up
Q8NC42	RNF149	E3 ubiquitin-protein ligase RNF149 OS = Homo sapiens OX = 9606 GN = RNF149	1.459	0.00037785	Up
P18510	IL1RN	Interleukin-1 receptor antagonist protein OS = Homo sapiens OX = 9606 GN = IL1RN	1.456	0.0024996	Up
Q7Z3E5	ARMC9	LisH domain-containing protein ARMC9 OS = Homo sapiens OX = 9606 GN = ARMC9	1.443	0.020124	Up
Q6PCB7	SLC27A1	Long-chain fatty acid transport protein 1 OS = Homo sapiens OX = 9606 GN = SLC27A1	1.428	0.023823	Up
Q08116	RGS1	Regulator of G-protein signaling 1 OS = Homo sapiens OX = 9606 GN = RGS1	1.428	0.0073823	Up
O43286	B4GALT5	"Beta-1,4-galactosyltransferase 5 OS = Homo sapiens OX = 9606 GN = B4GALT5"	1.412	0.00126306	Up
Q9Y624	F11R	Junctional adhesion molecule A OS = Homo sapiens OX = 9606 GN=F11R	1.399	0.00101647	Up
P53794	SLC5A3	Sodium/myo-inositol cotransporter OS = Homo sapiens OX = 9606 GN = SLC5A3	1.396	0.00834	Up
P07204	THBD	Thrombomodulin OS = Homo sapiens OX = 9606 GN = THBD	1.382	0.0023023	Up
Q9H0Q0	FAM49A	Protein FAM49A OS = Homo sapiens OX = 9606 GN = FAM49A	1.378	0.0046642	Up
Q5TGY3	AHDC1	AT-hook DNA-binding motif-containing protein 1 OS = Homo sapiens OX = 9606 GN = AHDC1	1.378	0.0088028	Up
P15090	FABP4	"Fatty acid-binding protein, adipocyte OS = Homo sapiens OX = 9606 GN = FABP4"	1.365	0.0095229	Up
Q16877	PFKFB4	"6-Phosphofructo-2-kinase/fructose-2,6-bisphosphatase 4 OS = Homo sapiens OX = 9606 GN = PFKFB4"	1.363	0.0045984	Up
Q58WW2	DCAF6	DDB1- and CUL4-associated factor 6 OS = Homo sapiens OX = 9606 GN = DCAF6	1.343	0.042763	Up
Q9UBN6	TNFRSF10D	Tumor necrosis factor receptor superfamily member 10D OS = Homo sapiens OX = 9606 GN = TNFRSF10D	1.336	0.032996	Up
P01033	TIMP1	Metalloproteinase inhibitor 1 OS = Homo sapiens OX = 9606 GN = TIMP1	1.333	0.0027818	Up
P60520	GABARAPL2	Gamma-aminobutyric acid receptor-associated protein-like 2 OS = Homo sapiens OX = 9606 GN = GABARAPL2	1.313	0.0052619	Up
Q9Y2Y9	KLF13	Krueppel-like factor 13 OS = Homo sapiens OX = 9606 GN = KLF13	1.304	0.0133835	Up
P04083	ANXA1	Annexin A1 OS = Homo sapiens OX = 9606 GN = ANXA1	1.302	0.0031812	Up

increased the expression of TNFSF9, TRAF1, p-ERK, IL-1β, and IL-6 ($P < 0.05$), except for p-AKT. In addition, the LPS-induced expression of TNFSF9 and TRAF1 was significantly lower when compared to the high concentration (400 μM) of the AI-2-treated group ($P < 0.05$). These findings indicated that AI-2 induced M1 polarization of macrophages possibly through a specific TNFSF9/TRAF1/p-AKT/IL-1β signaling pathway.

3.5. Increased TNFSF9 and IL-1β expression was associated with increased survival in human CRCs

Next, we explored whether the expression of TNFSF9/TRAF1/p-AKT/IL-1β was upregulated in human CRC tissues. TCGA and GTEx projects provided a large number of RNA sequencing data from human tumor tissue and normal tissue [28]. GEPIA (Gene Expression Profiling Interactive Analysis) is an online tool that is based on TCGA and GTEx data. Using the GEPIA database, we found that the mRNA expression of

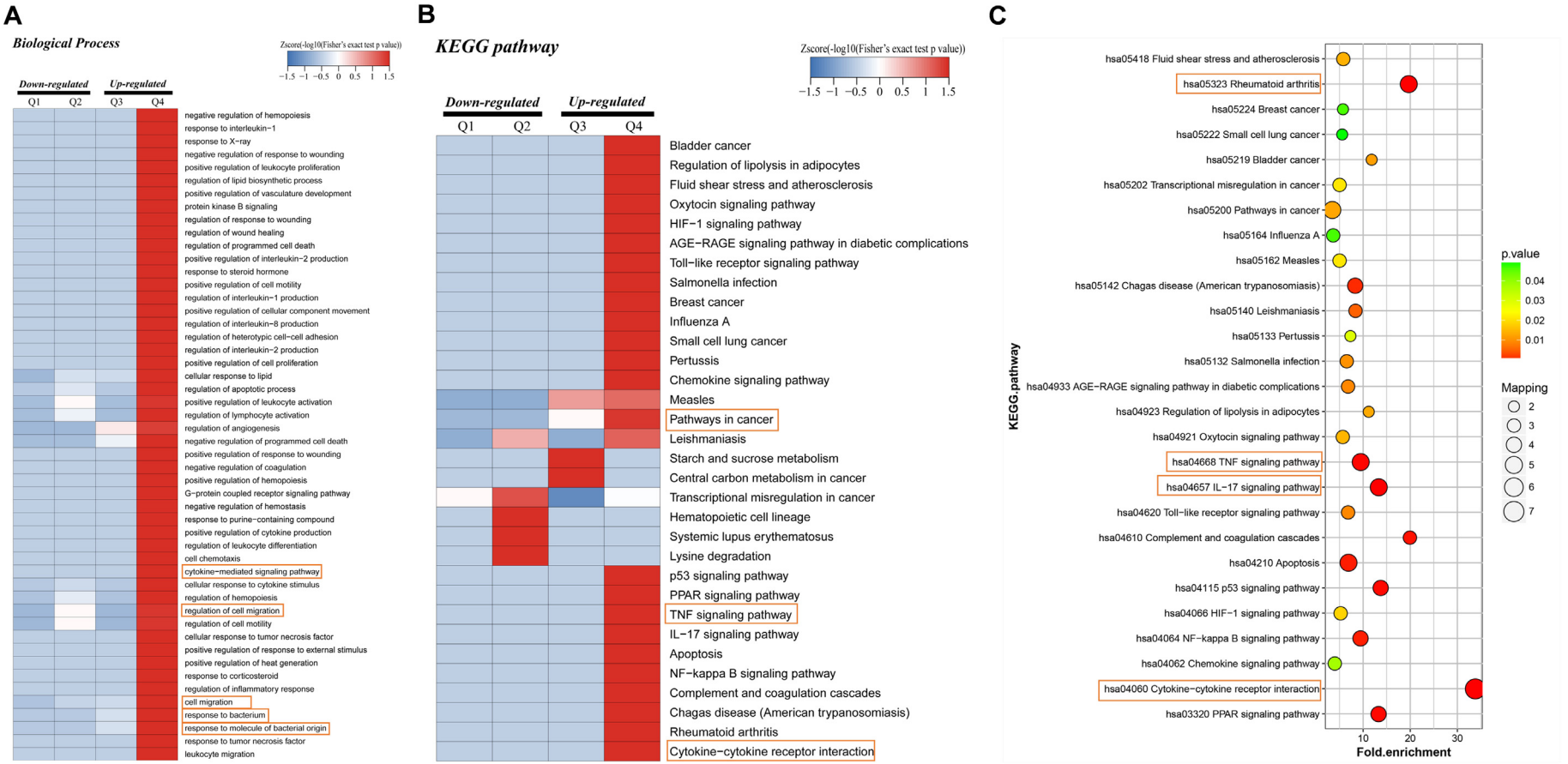

Fig. 3. Proteomic analysis of *Fusobacterium nucleatum* AI-2-treated U937-derived macrophages. (A) The differentially expressed proteins (a cutoff of absolute fold change ≥1.3 and P value < 0.05) in *Fusobacterium nucleatum* AI-2-treated macrophages when compared to the control were categorized according to the biological processes they were involved in. A series of biological processes related to the present study are highlighted in the box. (B, C) The differentially expressed proteins (a cutoff of absolute fold change ≥1.3 and P value < 0.05) in *Fusobacterium nucleatum* AI-2-treated macrophages when compared to the control were categorized according to the KEGG pathway they were involved in. Several KEGG pathways related to the study are presented in the box. Q1-Q2, downregulated proteins; Q1, 0 < Ratio ≤ 1/1.3 and P value < 0.05; Q2, 1/1.3 < Ratio ≤ 1/1.2 and P value < 0.05; Q3-Q4, upregulated proteins; Q3, 1.2 < Ratio ≤ 1.3 and P value < 0.05; Q4, Ratio > 1.3 and P value < 0.05.

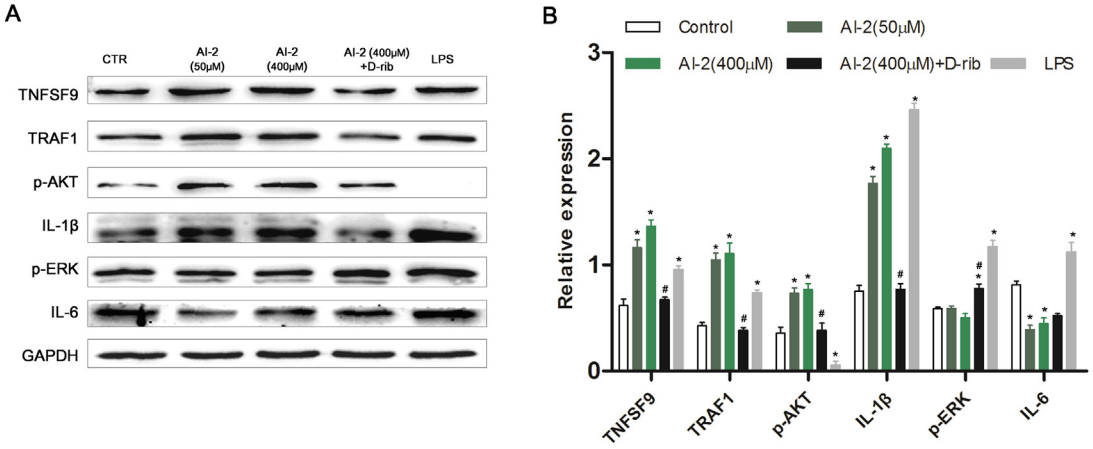

Fig. 4. *Fusobacterium nucleatum* AI-2 induced activation of TNFSF9/TRAF1/p-AKT/IL-1β signaling *in vitro*. (A, B) Western blots showing significantly increased protein levels of TNFSF9, TRAF1, p-AKT, and IL-1β in cultured U937-derived macrophages after *Fusobacterium nucleatum* AI-2 treatment when compared to the control group. TNFSF9, TRAF1, p-AKT, and IL-1β protein levels were significantly decreased in the D-ribose (50 μM) pre-treatment group when compared to the AI-2 treatment group. IL-6 expression was significantly decreased in AI-2-challenged macrophages when compared to the control group. LPS significantly increased the expression of TNFSF9, TRAF1, IL-1β, p-ERK, and IL-6 but not p-AKT when compared to control group. Bar diagrams represent the results obtained after densitometric scanning from three different experiments. Bars represent the mean ± SD. $P < 0.05$ compared to the control group, $\#P < 0.05$ compared to the AI-2 (400 μM) group. AI-2, autoinducer-2; D-rib, D-ribose.

TNFSF9 and IL-1β was significantly higher in CRCs (n = 275) when compared to NCs (n = 349) ($P < 0.05$, Fig. 5). In addition, the mRNA expression of TRAF1, p-AKT, p-ERK, and IL-6 did not significantly differ between groups. Interestingly, CRC patients with a high expression of IL-1β had a significantly better overall survival when compared to patients with a low IL-1β expression ($P < 0.05$). Furthermore, CRC patients with a high expression of TNFSF9 had a better survival compared to patients with a low TNFSF9 expression, although this difference was not significant ($P > 0.05$) (Fig. 5).

To prove the cell source of TNFSF9 and IL-1β in CRC microenvironment, multi-immunofluorescence was performed to analyze the co-staining of macrophages (CD68) and TNFSF9/IL-1β in 23 CRCs with low AI-2 concentration and 17 CRCs with high AI-2 concentration in stool. The co-staining of macrophages ($CD68^+$) and TNFSF9/IL-1β protein was frequently seen in CRC tissues (Fig. 6A, C). In addition, the frequency of co-staining for $CD68^+$ macrophages and TNFSF9/IL-1β protein in CRCs with high AI-2 concentration was significantly higher when compared to that with low AI-2 concentration in stool (both $P < 0.0001$) (Fig. 6A–D). These findings suggested that macrophages are a major source of increased TNFSF9/IL-1β expression in human CRC tissues, which was associated with high AI-2 concentration in the gut.

4. Discussion

The phenotype of macrophages can be shaped by the microenvironment, and M1 type polarization is pro-inflammatory and has an anti-tumor effect [13]. We purified AI-2 from *F. nucleatum* (*F01*) strains, which were isolated from proximal colon cancer tissue in our previous study [23]. To the best of our knowledge, the levels of AI-2 in the intestine are unknown. In the present study, we selected 50 μM AI-2, which was used in a previous interkingdom study, and selected 400 μM AI-2 as the high concentration as used previously [29]. In addition, the AI-2 inhibitor D-ribose significantly inhibited AI-2-induced bioluminescence. We showed for the first time that AI-2 from *F. nucleatum* (*F01*) promoted M1 polarization and migration of cultured U937-derived macrophages *in vitro*. These findings suggested that AI-2 purified from *F. nucleatum* (*F01*) may activate macrophages, thereby promoting inflammatory responses and anti-tumor immunity.

In a previous study, it was revealed that non-pathogenic *Escherichia coli* AI-2 induced the release of various inflammatory factors, such as IL-8 and TNF in colon cancer cells [29]. Because macrophages have an important role in microbial sensing [12], we analyzed AI-2-interacting proteins in macrophages using a quantitative proteomics approach. Forty-six proteins were up-regulated with expression levels that were changed > 1.3-fold, primarily including inflammatory cytokines, such as TNFSF9, IL-1β, CCL20, PTGS2, TRAF1, and CCL3. The most significantly upregulated proteins included TNFSF9 and IL-1β (expression levels > 3-fold change). Thus, *F. nucleatum* AI-2 may activate macrophages by inducing the release of inflammatory cytokines mainly involving TNFSF9 and IL-1β.

The metabolites of gut microbiota can induce changes in the signaling pathways of the host [30]. We found for the first time that *F. nucleatum* AI-2 induced macrophage M1 polarization possibly through the TNFSF9/TRAF1/p-AKT/IL-1β signaling pathway. It was found that TNFSF9 signaling induced IL-1β expression, and AKT activation is critical for TNFSF9-mediated IL-1β expression [31]. Moreover, TRAF1 is critical in TNFSF9-dependent memory T cell survival and expansion [32,33]. Therefore, our results were consistent with these findings.

In human CRC tissue, we found that the expression of TNFSF9 and IL-1β was significantly higher compared to that in normal tissue. Moreover, our analysis showed that CRC patients with high levels of TNFSF9 and IL-1β had a better survival than patients with a low expression. It has been reported that TNFSF9 can activate dendritic cells, inducing CD8+ T cells to a Tc1 phenotype by secreting IL-1β, resisting tumor-associated viruses, such as EBV and HBV [34,35]. Moreover, TNFSF9 possessed an unequaled capacity for pro-inflammatory polarization of anti-tumor lymphocytes [36]. In another study, it was shown that TNFSF9 significantly inhibited the proliferation, migration, and invasion of hepatocellular carcinoma cells *in vitro* or *vivo*, thereby exerting an anti-tumor immunity [37]. In previous studies, it was found that not all IL-1β signaling is involved in tumor promotion, and IL-1β is capable of stimulating caspase-11 expression, thereby mediating tumor suppressing activities of STAT1 in intestinal epithelial cells [38]. IL-1β can contribute to the protective effect of MyD88 during colitis-associated cancer, and the physiological levels of IL-1 are essential for anti-tumor immunity [39,40]. In addition, the results in present study suggested that macrophages are a major source of increased TNFSF9/IL-1β expression in human CRC tissues, which was associated with high AI-2 concentration in the gut. Taken together, these findings suggested that *F. nucleatum* AI-2 may have an anti-tumor effect by activating TNFSF9/IL-1β signaling in macrophages.

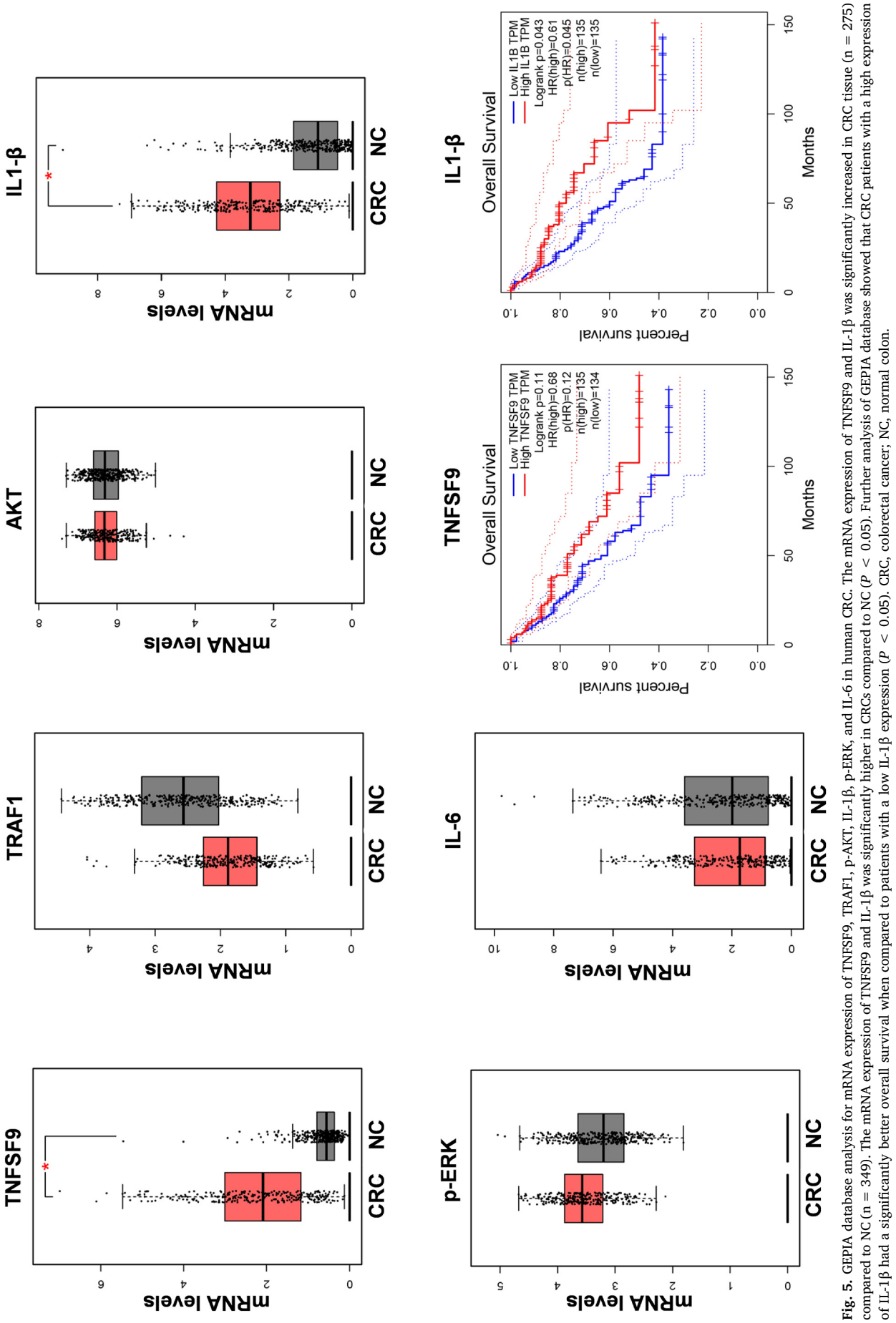

Fig. 5. GEPIA database analysis for mRNA expression of TNFSF9, TRAF1, p-AKT, IL-1β, p-ERK, and IL-6 in human CRC. The mRNA expression of TNFSF9 and IL-1β was significantly increased in CRC tissue (n = 275) compared to NC (n = 349). The mRNA expression of TNFSF9 and IL-1β was significantly higher in CRCs compared to NC ($P < 0.05$). Further analysis of GEPIA database showed that CRC patients with a high expression of IL-1β had a significantly better overall survival when compared to patients with a low IL-1β expression ($P < 0.05$). CRC, colorectal cancer; NC, normal colon.

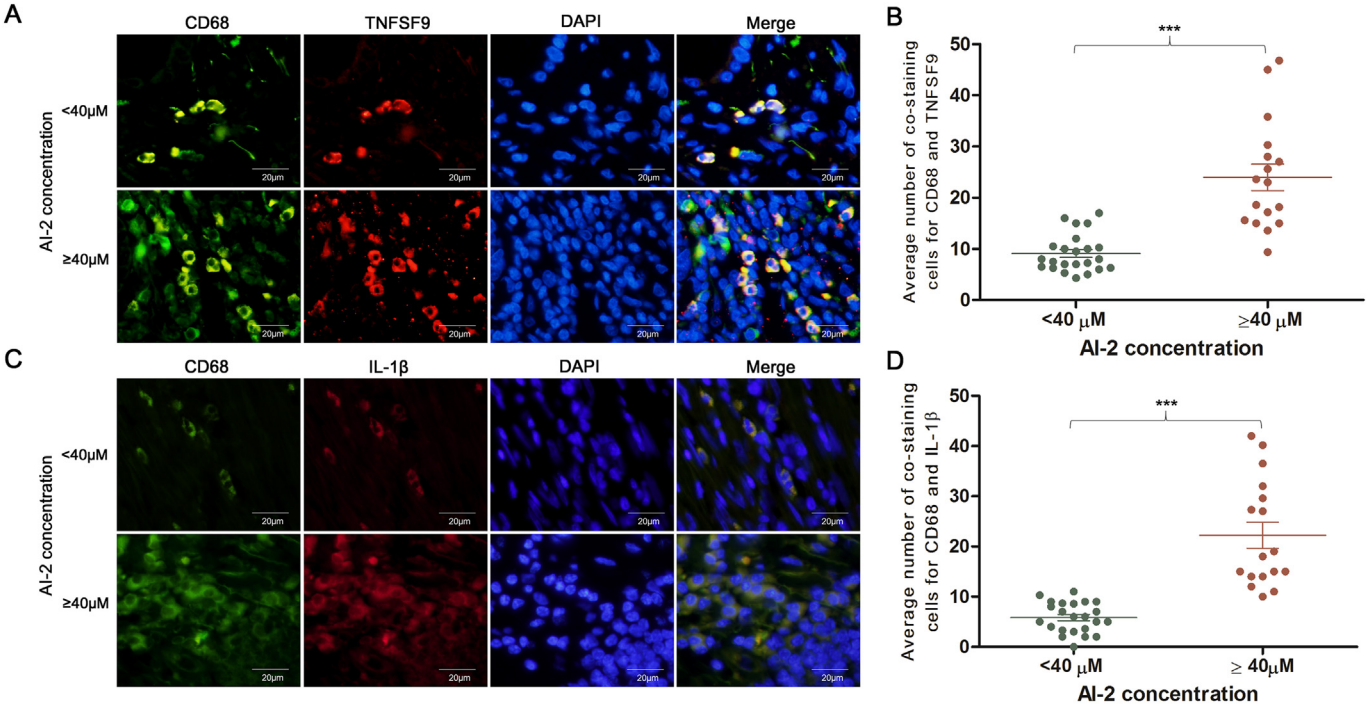

Fig. 6. The co-staining of macrophages and TNFSF9/IL-1β in human colorectal cancer correlating to autoinducer-2 concentration. (A, C) Representative images of co-staining for macrophages ($CD68^+$) and $TNFSF9^+$/IL-1β in colorectal cancer (CRC) tissues. (B, D) The frequency of co-staining for $CD68^+$ macrophages and TNFSF9/IL-1β protein in CRCs with high AI-2 concentration was significantly higher when compared to that with low AI-2 concentration in stool (both $P < 0.0001$). Magnification, 400×; scale bars, 20 μm. AI-2, autoinducer-2. ***$P < 0.001$.

F. nucleatum is a pathogenic bacteria contributing to the carcinogenesis of CRC [16]. In our previous study as well as in studies by others it has been shown that *F. nucleatum* promoted M2 polarization of macrophages in the microenvironment of colorectal tumors [14,41]. On the contrary, in the present study, AI-2 from *F. nucleatum* induced macrophage M1 polarization. The virulence of *F. nucleatum* includes a variety of virulent factors, such as LPS, FadA, Fap2, and RadD [17], which can contribute to the development of CRC either together or alone. Moreover, in the present study, macrophages were challenged by AI-2 for a short period (6 h) *in vitro*. Therefore, whether AI-2 from gut *F. nucleatum* has a similar effect on macrophages *in vivo* needs to be elucidated.

AI-2 is a nonspecies-specific autoinducer that mediates the communication among interspecies, and its levels modulate the abundance of major phyla of intestinal microbiota [10]. Increased AI-2 levels can partially reverse intestinal dysbiosis caused by streptomycin through expansion of *Firmicutes* and reduction of *Bacteroidetes* [42]. Therefore, it is conceivable that AI-2 may change the density and composition of intestinal flora, thereby providing a novel regulator of gut microbiota. Taken together, our data suggested that AI-2 induced macrophage M1 polarization by activating the TNFSF9/TRAF1/p-AKT/IL-1β pathway, to play a pro-inflammatory role and have an anti-tumor effect. Thus, AI-2 may serve as a promising novel target for immunotherapy of gut microbiota-related diseases.

Supplementary data to this article can be found online at https://doi.org/10.1016/j.intimp.2019.105724.

Funding

This work was supported by Natural Science Foundation of Sichuan Science and Technology Agency, Chengdu City, China, under Award, No. 2018JY0167.

Author contribution

JW, KL, WP, QL, HL, YR, YP and XT conducted the experiments. JW, WP and YP analyzed the data. XF wrote the paper. XF conceived and designed the study.

Declaration of Competing Interest

All authors declare no financial disclosures and no conflict of interest.

Acknowledgements

We would like to acknowledge the Central Laboratory of Southwestern Medical University for providing facilities for this experiment.

References

[1] V. Sethi, S. Kurtom, M. Tarique, S. Lavania, Z. Malchiodi, L. Hellmund, L. Zhang, U. Sharma, B. Giri, B. Garg, et al., Gut microbiota promotes tumor growth in mice by modulating immune response, Gastroenterology 155 (2018) 33–37 e6.
[2] G. Rook, F. Bäckhed, B.R. Levin, M.J. McFall-Ngai, A.R. McLean, Evolution, human-microbe interactions, and life history plasticity, Lancet 390 (2017) 521–530.
[3] P. Maruvada, V. Leone, L.M. Kaplan, E.B. Chang, The human microbiome and obesity: moving beyond associations, Cell Host Microbe 22 (2017) 589–599.
[4] K. Forslund, F. Hildebrand, T. Nielsen, G. Falony, E. Le Chatelier, S. Sunagawa, E. Prifti, S. Vieira-Silva, V. Gudmundsdottir, H.K. Pedersen, et al., Disentangling type 2 diabetes and metformin treatment signatures in the human gut microbiota, Nature 528 (2015) 262–266.
[5] Z. Jie, H. Xia, S.L. Zhong, Q. Feng, S. Li, S. Liang, H. Zhong, Z. Liu, Y. Gao, H. Zhao, et al., The gut microbiome in atherosclerotic cardiovascular disease, Nat. Commun. 8 (2017) 845.
[6] M.Y. Zeng, N. Inohara, G. Nunez, Mechanisms of inflammation-driven bacterial dysbiosis in the gut, Mucosal Immunol. 10 (2017) 18–26.
[7] A. Dzutsev, J. H. Badger, E. Perez-Chanona, S. Roy, R. Salcedo, C. K. SmithandG. Trinchieri, Microbes and Cancer, Annu. Rev. Immunol. 35 (2017) 199–228.
[8] J.B. Kaper, V. Sperandio, Bacterial cell-to-cell signaling in the gastrointestinal tract, Infect. Immun. 73 (2005) 3197–3209.
[9] S. Moreno-Gamez, R.A. Sorg, A. Domenech, M. Kjos, F.J. Weissing, G.S. van

Doornand, J.W. Veening, Quorum sensing integrates environmental cues, cell density and cell history to control bacterial competence, Nat. Commun. 8 (2017) 854.
[10] J.A. Thompson, R.A. Oliveira, A. Djukovic, C. Ubeda, K.B. Xavier, Manipulation of the quorum sensing signal AI-2 affects the antibiotic-treated gut microbiota, Cell Rep. 10 (2015) 1861–1871.
[11] N. Scheres, R.J. Lamont, W. Crielaardand, B.P. Krom, LuxS signaling in Porphyromonas gingivalis-host interactions, Anaerobe 35 (2015) 3–9.
[12] A. Mortha, A. Chudnovskiy, D. Hashimoto, M. Bogunovic, S.P. Spencer, Y. Belkaidand, M. Merad, Microbiota-dependent crosstalk between macrophages and ILC3 promotes intestinal homeostasis, Science 343 (2014) 1249288.
[13] F.O. Martinez, L. Helming, S. Gordon, Alternative activation of macrophages: an immunologic functional perspective, Annu. Rev. Immunol. 27 (2009) 451–483.
[14] T. Chen, Q. Li, J. Wu, Y. Wu, W. Peng, H. Li, J. Wang, X. Tang, Y. Peng, X. Fu, Fusobacterium nucleatum promotes M2 polarization of macrophages in the microenvironment of colorectal tumours via a TLR4-dependent mechanism, Cancer Immunol. Immunother. 67 (2018) 1635–1646.
[15] J. Zhong, H. Wang, W. Chen, Z. Sun, J. Chen, Y. Xu, M. Weng, Q. Shi, D. MaandC. Miao, Ubiquitylation of MFHAS1 by the ubiquitin ligase praja2 promotes M1 macrophage polarization by activating JNK and p38 pathways, Cell Death Dis. 8 (2017) e2763.
[16] C.L. Sears, The who, where and how of fusobacteria and colon cancer, Elife 7 (2018).
[17] Y.W. Han, Fusobacterium nucleatum: a commensal-turned pathogen, Curr. Opin. Microbiol. 23 (2015) 141–147.
[18] S. Afrin, F. Giampieri, M. Gasparrini, T.Y. Forbes-Hernandez, D. Cianciosi, P. Reboredo-Rodriguez, J. Zhang, P.P. Manna, M. Daglia, A.G. Atanasov, et al., Dietary phytochemicals in colorectal cancer prevention and treatment: a focus on the molecular mechanisms involved, Biotechnol. Adv. 18 (2018) 30195–30202.
[19] Y. Sun, Y. Zhao, X. Wang, L. Zhao, W. Li, Y. Ding, L. Kong, Q. Guoand, N. Lu, Wogonoside prevents colitis-associated colorectal carcinogenesis and colon cancer progression in inflammation-related microenvironment via inhibiting NF-kappaB activation through PI3K/Akt pathway, Oncotarget 7 (2016) 34300–34315.
[20] G. Wang, Y. Ye, X. Zhang, J. Song, Bradykinin stimulates IL-6 production and cell invasion in colorectal cancer cells, Oncol. Rep. 32 (2014) 1709–1714.
[21] N. Sanapareddy, R.M. Legge, B. Jovov, A. McCoy, L. Burcal, F. Araujo-Perez, T.A. Randall, J. Galanko, A. Benson, R.S. Sandler, et al., Increased rectal microbial richness is associated with the presence of colorectal adenomas in humans, ISME J 6 (2012) 1858–1868.
[22] N. Raut, P. Pasiniand, S. Daunert, Deciphering bacterial universal language by detecting the quorum sensing signal, autoinducer-2, with a whole-cell sensing system, Anal. Chem. 85 (2013) 9604–9609.
[23] Y. Chen, Y. Peng, J. Yu, T. Chen, Y. Wu, L. Shi, Q. Li, J. Wuand, X. Fu, Invasive fusobacterium nucleatum activates beta-catenin signaling in colorectal cancer via a TLR4/P-PAK1 cascade, Oncotarget 8 (2017) 31802–31814.
[24] R. Vilchez, A. Lemme, V. Thiel, S. Schulz, H. Sztajer, I. Wagner-Dobler, Analysing traces of autoinducer-2 requires standardization of the Vibrio harveyi bioassay, Anal. Bioanal. Chem. 387 (2007) 489–496.
[25] V. Sperandio, A.G. Torres, B. Jarvis, J.P. Nataro, J.B. Kaper, Bacteria-host communication: the language of hormones, Proc. Natl. Acad. Sci. U. S. A. 100 (2003) 8951–8956.
[26] H. Kitamura, T. Nakagawa, M. Takayama, Y. Kimura, A. Hijikataand, O. Ohara, Post-transcriptional effects of phorbol 12-myristate 13-acetate on transcriptome of U937 cells, FEBS Lett. 578 (2004) 180–184.
[27] C.Y. Chen, S.S. Rao, L. Ren, X.K. Hu, Y.J. Tan, Y. Hu, J. Luo, Y.W. Liu, H. Yin, J. Huang, et al., Exosomal DMBT1 from human urine-derived stem cells facilitates diabetic wound repair by promoting angiogenesis, Theranostics 8 (2018) 1607–1623.
[28] Z. Tang, C. Li, B. Kang, G. Gao, C. Liand, Z. Zhang, GEPIA: a web server for cancer and normal gene expression profiling and interactive analyses, Nucleic Acids Res. 45 (2017) W98–W102.
[29] A. Zargar, D. N. Quan, K. K. Carter, M. Guo, H. O. Sintim, G. F. PayneandW. E. Bentley, Bacterial secretions of nonpathogenic Escherichia coli elicit inflammatory pathways: a closer investigation of interkingdom signaling, MBio 6 (2015) e00025.
[30] C.A. Lozupone, J.I. Stombaugh, J.I. Gordon, J.K. Jansson, R. Knight, Diversity, stability and resilience of the human gut microbiota, Nature 489 (2012) 220–230.
[31] D. K. Kim, S. C. LeeandH. W. Lee, CD137 ligand-mediated reverse signals increase cell viability and cytokine expression in murine myeloid cells: involvement of mTOR/p70S6 kinase and Akt, Eur. J. Immunol. 39 (2009) 2617–2628.
[32] T.H. Watts, G.H. Lin, C. Wang, A.J. McPherson, L.M. Snelland, L. Sabbagh, Role of 4-1BBL and TRAF1 in the CD8 T cell response to influenza virus and HIV, Adv. Exp. Med. Biol. 691 (2011) 177–186.
[33] C. Wang, T. Wen, J. P. Routy, N. F. Bernard, R. P. SekalyandT. H. Watts, 4-1BBL induces TNF receptor-associated factor 1-dependent Bim modulation in human T cells and is a critical component in the costimulation-dependent rescue of functionally impaired HIV-specific CD8 T cells, J. Immunol. 179 (2007) 8252–8263.
[34] B. Dharmadhikari, E. Nickles, Z. Harfuddin, N.D.B. Ishak, Q. Zeng, A. Bertolettiand, H. Schwarz, CD137L dendritic cells induce potent response against cancer-associated viruses and polarize human CD8(+) T cells to Tc1 phenotype, Cancer Immunol. Immunother. 67 (2018) 893–905.
[35] C. Lee-Chang, M. Bodogai, K. Moritoh, P.B. Olkhanud, A.C. Chan, M. Croft, J.A. Mattison, P.J. Holst, R.E. Gress, L. Ferrucci, et al., Accumulation of 4-1BBL+ B cells in the elderly induces the generation of granzyme-B+ CD8+ T cells with potential antitumor activity, Blood 124 (2014) 1450–1459.
[36] T. Bartkowiak, M.A. Curran, 4-1BB agonists: multi-potent Potentiators of tumor immunity, Front. Oncol. 5 (2015) 117.
[37] Y.L. Shen, Y. Gan, H.F. Gao, Y.C. Fan, Q. Wang, H. Yuan, Y.F. Song, J.D. Wang, H. Tu, TNFSF9 exerts an inhibitory effect on hepatocellular carcinoma, J. Dig. Dis. 18 (2017) 395–403.
[38] B. Flood, J. Manils, C. Nulty, E. Flis, S. Kenealy, G. Barber, J. Fay, K.H.G. Mills, E.W. Kay, E.M. Creagh, Caspase-11 regulates the tumour suppressor function of STAT1 in a murine model of colitis-associated carcinogenesis, Oncogene 38 (2018) 2658–2674.
[39] R. Salcedo, A. Worschech, M. Cardone, Y. Jones, Z. Gyulai, R.M. Dai, E. Wang, W. Ma, D. Haines, C. O'HUigin, et al., MyD88-mediated signaling prevents development of adenocarcinomas of the colon: role of interleukin 18, J. Exp. Med. 207 (2010) 1625–1636.
[40] Y. Carmi, G. Rinott, S. Dotan, M. Elkabets, P. Rider, E. Voronov, R.N. Apte, Microenvironment-derived IL-1 and IL-17 interact in the control of lung metastasis, J. Immunol. 186 (2011) 3462–13471.
[41] H.E. Park, J.H. Kim, N.Y. Cho, H.S. Lee, G.H. Kang, Intratumoral fusobacterium nucleatum abundance correlates with macrophage infiltration and CDKN2A methylation in microsatellite-unstable colorectal carcinoma, Virchows Arch. 471 (2017) 329–336.
[42] Z. Sun, V. Grimmand, C.U. Riedel, AI-2 to the rescue against antibiotic-induced intestinal dysbiosis? Trends Microbiol. 23 (2015) 327–328.